Radiology

REVIEWS AND COMMENTARY • REVIEW

Musculoskeletal CT Imaging: State-of-the-Art Advancements and Future Directions

Shadpour Demehri, MD • Francis I. Baffour, MD • Joshua G. Klein, BS • Elena Ghotbi, MD • Hamza Ahmed Ibad, MD • Kamyar Moradi, MD • Katsuyuki Taguchi, PhD, MSc • Jan Fritz, MD • John A. Carrino, MD, MPH • Ali Guermazi, MD, PhD • Elliot K. Fishman, MD • Wojciech B. Zbijewski, PhD

From the Russell H. Morgan Department of Radiology and Radiological Science (S.D., J.G.K., E.G., H.A.I., K.M., K.T., E.K.F.) and Department of Biomedical Engineering (W.B.Z.), Johns Hopkins University School of Medicine, 601 N Carolina St, Baltimore, MD 21287; Division of Musculoskeletal Imaging, Department of Radiology, Mayo Clinic, Rochester, Minn (F.I.B.); Department of Radiology, New York University Grossman School of Medicine, New York, NY (J.F.); Department of Radiology and Imaging, Hospital for Special Surgery, New York, NY (J.A.C.); and Department of Radiology, Quantitative Imaging Center, Boston University School of Medicine, Boston, Mass (A.G.).
Received February 10, 2023; revision requested March 27; revision received April 28; accepted May 15. **Address correspondence to** S.D. (email: *demehri2001@yahoo.com*).

Conflicts of interest are listed at the end of this article.

See also the review "MRI Advancements in Musculoskeletal Clinical and Research Practice" by Sneag et al in this issue.

Radiology 2023; 308(2):e230344 • https://doi.org/10.1148/radiol.230344 • Content codes: MK CT

CT is one of the most widely used modalities for musculoskeletal imaging. Recent advancements in the field include the introduction of four-dimensional CT, which captures a CT image during motion; cone-beam CT, which uses flat-panel detectors to capture the lower extremities in weight-bearing mode; and dual-energy CT, which operates at two different x-ray potentials to improve the contrast resolution to facilitate the assessment of tissue material compositions such as tophaceous gout deposits and bone marrow edema. Most recently, photon-counting CT (PCCT) has been introduced. PCCT is a technique that uses photon-counting detectors to produce an image with higher spatial and contrast resolution than conventional multidetector CT systems. In addition, postprocessing techniques such as three-dimensional printing and cinematic rendering have used CT data to improve the generation of both physical and digital anatomic models. Last, advancements in the application of artificial intelligence to CT imaging have enabled the automatic evaluation of musculoskeletal pathologies. In this review, the authors discuss the current state of the above CT technologies, their respective advantages and disadvantages, and their projected future directions for various musculoskeletal applications.

Currently, more than 80 million CT examinations are performed annually in the United States (1), approximately 8 million of which are conducted for musculoskeletal indications (2). The last fundamental breakthrough in CT technology occurred approximately 30 years ago when the concept of continuous "helical CT" was introduced, which improved CT technology by replacing the "one section at a time" acquisition mode with continuous patient translation (3). Since then, there have been tremendous advancements in CT technology, including gradual improvements in detectors and innovative approaches to mitigating the associated increase in radiation exposure (Table). In 2008, large-bore 320–detector row multidetector CT (MDCT) with 16-cm wide-area coverage was developed. This eliminated "stair-step" artifacts inherent in 64-section technology during cardiothoracic imaging and provided a platform for four-dimensional (4D) kinematic CT imaging of the peripheral joints (4). Along with advances in MDCT detector systems, the concept of simultaneous acquisition of dual-energy CT (DECT) scans was developed, with two x-ray tubes being operated at two different tube potentials (5). In the past decade, cone-beam CT (CBCT) has also been established and has made the availability of three-dimensional (3D) high-resolution imaging of lower extremities in weight-bearing mode feasible (6). First approved for clinical use in 2021, photon-counting CT (PCCT) represents the most recent innovation in CT technology. It uses photon-counting detectors (PCDs) to measure x-ray projections in comparatively higher quality than widespread energy-integrating detectors (EIDs) for MDCT (7). By converting individual x-ray photons into a charge cloud and bypassing the electronic noise–inducing steps associated with EID signal aggregation, PCCT can achieve markedly higher contrast resolution.

In addition to image acquisition, there have been advancements in image postprocessing. Cinematic rendering is a novel postprocessing visualization technique that uses innovative lighting models to generate an image from CT data (8). Cinematic rendering reconstructions have shown superior illustrative quality than volume rendering reconstructions in some musculoskeletal pathologies (9). Three-dimensional printing technology has also shown clinical utility in producing patient-specific anatomic models. Although 3D printing has been primarily used for preoperative planning, ongoing research is focused on generating 3D-printed tissue replacements for use in grafts. Finally, the application of artificial intelligence and automated evaluation of musculoskeletal CT images is an emerging field of research. In this article, we review recent advancements in musculoskeletal CT imaging and provide future directions for each CT technology.

Four-dimensional CT

Principle

Four-dimensional CT is a high-resolution volumetric acquisition of a peripheral joint during motion, which includes the fourth dimension (ie, time). In the past 3

Abbreviations

CBCT = cone-beam CT, DECT = dual-energy CT, EID = energy-integrating detector, 4D = four-dimensional, MDCT = multidetector CT, PCCT = photon-counting CT, PCD = photon-counting detector, 3D = three-dimensional

Summary

CT currently enables musculoskeletal examinations during motion and weight-bearing with high resolution; the recent advancement of photon-counting CT will further improve musculoskeletal imaging at a reduced radiation exposure.

Essentials

- Four-dimensional CT captures dynamic images of peripheral joints during motion.
- Dual-energy CT generates two spatially matching CT data sets with two sufficiently different tube energies, which can provide spectral differentiation of soft-tissue and osseous materials and molecular substrates.
- Cone-beam CT uses flat-panel detectors to perform three-dimensional high-resolution imaging of the lower extremities in weight-bearing mode.
- High-resolution peripheral quantitative CT is a low-dose modality used to access bone microarchitecture and density; high-spatial-resolution CT is characterized by a detector with a pixel size of 250 μm^2, allowing for improved visualization of trabecular bone microarchitecture in the axial skeleton.
- Photon-counting CT uses novel photon-counting detectors to produce high contrast resolution for bone and soft tissue.

decades (10), the use of large-bore 320-detector MDCT has made this method feasible in clinical practice. With use of predefined imaging acquisition protocols, patients can be trained to perform peripheral joint motions before CT acquisition to help detect and characterize their dynamic biomechanical derangements. Due to the large volume of data acquired during each 4D CT examination, diligence during the procedure is crucial to minimize radiation exposure without compromising image resolution. With use of iterative reconstruction techniques, the 4D CT examinations can be performed at a reduced noise with low radiation exposure while preserving spatial resolution and contrast (11).

Due to multiple consecutive CT acquisitions during the joint motion, 4D CT acquisitions are associated with higher cumulative radiation exposure compared with MDCT (12). However, the skin is the only radiation-sensitive tissue in 4D CT examinations of the distal peripheral joints. Therefore, despite the increased cumulative radiation exposure, the effective radiation dose associated with 4D CT examinations of the distal peripheral joints remains relatively low.

Clinical Utility

The patellofemoral joint is the most investigated peripheral joint in the clinical application of 4D CT. Using 4D CT, radiologists can now characterize its biomechanical derangements and study the relationship between patellofemoral instability and patterns of patellofemoral maltracking during flexion-extension motion (Fig 1) (13). In addition, 4D CT can help evaluate corrective patellofemoral surgery outcomes; the ability to study patellar tracking in vivo also allows the orthopedist to access postoperative joint movement during active motion (14). To evaluate the outcome of medial patellofemoral ligament reconstruction surgery, researchers have imaged the knee joint over approximately 21 consecutive volumetric acquisitions over 10 seconds during

Overview of the Characteristics of Available CT Technologies for Musculoskeletal Applications

CT Type	First Introduction into Clinical Practice	Radiation Exposure (compared with MDCT)	Resolution (compared with MDCT)	Kinematic Imaging	Weight-bearing Imaging	Dual and/or Multi-energy Image Acquisition
Four-dimensional CT	2009 (87)	Cumulative radiation exposure: high Effective dose: low*	Resolution comparable with MDCT	Yes	No	No
Dual-energy CT	2006 (88)	High (89)	Spectral differentiation of materials and molecular substrates; specialized image reconstruction	No	No	Yes
Extremity cone-beam CT	2014 (6)	Medium (94)	High spatial resolution (0.26 × 0.26 mm) (6)	No	Yes	No
High-resolution peripheral quantitative CT	2005 (66)	Medium	High spatial resolution (0.1 × 0.1 mm to 0.14 × 0.14 mm) (67)	No	No	No
High-spatial-resolution CT	2017 (73)	High (71)	0.4 × 0.5 mm^2 (72)	No	No	No
Photon-counting CT	Past decade (first FDA approval in the United States: 2021) (90)	Medium (91)	High contrast resolution for bone and soft tissue Better spatial resolution (0.27 × 0.32 mm^2) (91)	No	No	Yes

Note.—MDCT = multidetector CT, FDA = U.S. Food and Drug Administration.

* Equal to or less than that of an average head CT examination (2 mSv) (12).

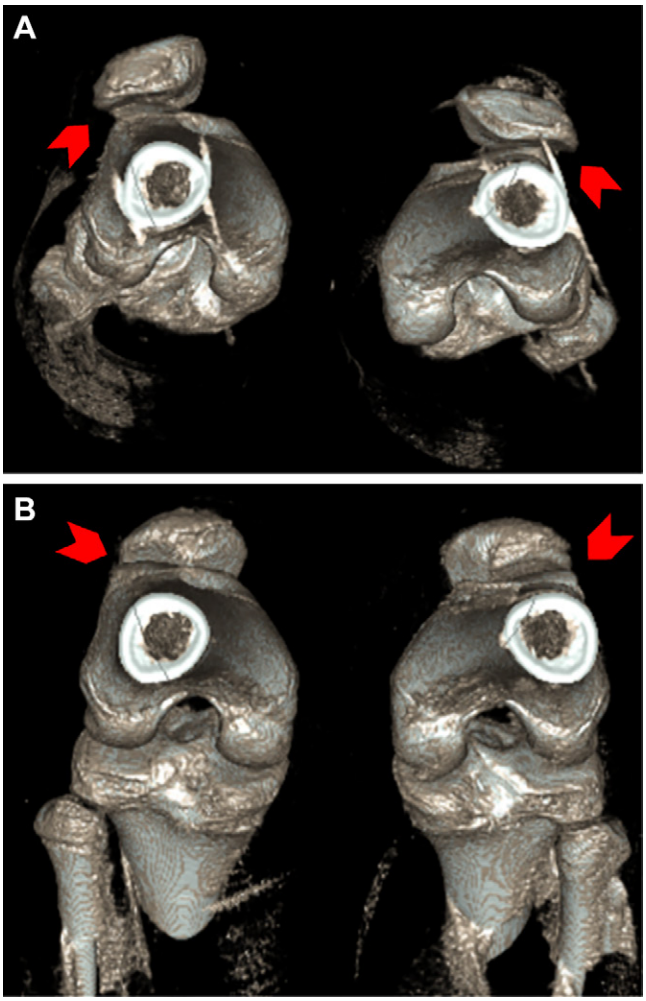

Figure 1: Four-dimensional CT scans in a 14-year-old female patient with patellofemoral maltracking. **(A)** Images obtained in full extension show subluxation of the patella with a "J-shape" patellofemoral maltracking pattern (arrowheads). **(B)** Subluxation is not seen (arrowheads) on images obtained full flexion (arrowheads).

active motion of the knee from 90° flexion to full extension, without an applied load (14).

Given the kinematic and structural complexity of ankle joints, 4D CT assessment of biomechanical derangements can provide benefits over traditional clinical examinations. This method can also replace two-dimensional radiographic measurements of ankle instabilities and syndesmotic injuries by tracking measurements during active motion (15). In one study (15), imaging of the ankle was conducted by performing 11 consecutive acquisitions over 5 seconds while actively moving the ankle from plantarflexion to dorsiflexion without an applied load. Investigations have also shown the potential for evaluating subtalar joint immobilization devices and ligament reconstruction effectiveness through 4D CT (16).

Akin to ankle joints, the wrist represents another complex joint for which 4D CT can provide added diagnostic value. Indeed, 4D CT has been used to investigate the corrective effect of surgical scapholunate ligament repair and carpal kinematic instabilities associated with a scapholunate interosseous ligament injury (17,18). To study surgical scapholunate ligament repair, one study performed 11 consecutive acquisitions over 5 seconds during active wrist motion without an applied load for a number of movements, including active clenching of the fist and deviating the wrist from the radial to ulnar sides (17). Furthermore, the prospective Accuracy of 4D CT for Diagnosing Instable Scapholunate Dissociation, or ACTION, trial has been recently designed with the primary aim of establishing the potential role of 4D CT in diagnosing scapholunate ligament injuries (19). Dynamic ulnocarpal abutment can also be shown using 4D CT in patients with diffuse wrist pain, and adequate repair and kinematic stability can be confirmed using postoperative 4D CT examinations (18). To our knowledge, there has been no study directly comparing the diagnostic performance of 4D CT with dynamic fluoroscopy. However, 4D CT will probably be advantageous over traditional dynamic fluoroscopy due to the high spatial resolution and feasibility of 3D imaging acquisition, which could improve detailed biomechanical assessment compared with conventional two-dimensional fluoroscopy.

It should be noted that 4D CT has been successfully used to image pathologies in other proximal joints, such as the shoulder and hip (20,21). However, the exponential increase of radiation dose exposure from 4D CT scans as compared with conventional MDCT scans must be taken into consideration given the close proximity of the hip and shoulder joints to radiation-sensitive organs (eg, ovaries and testicles, breast, and thyroid gland).

Advantages and Disadvantages

Four-dimensional CT is particularly suited for the kinematic imaging of joints compared with conventional CT, providing insight into the peripheral joint biomechanical instabilities. However, 4D CT is associated with a higher effective radiation dose than MDCT, and radiation exposure must be carefully considered and monitored.

Future Directions

Consistent with prior advancements, continued developments in temporal resolution will enable improved 4D CT image quality during motion while decreasing scanning times and radiation exposure. Such improvements could also expand the application of 4D CT technology to other anatomic locations (22). Kinematic assessment of robust 4D CT examination data using postprocessing software could be investigated in future studies for the characterization of biomechanical derangements and their improvements following corrective surgeries, and for risk stratification of posttraumatic secondary osteoarthritis (15). Future challenges include motion artifacts, metal artifacts from implants, concerns about radiation exposure, and large data sets requiring substantial time and effort for image processing. Advancements in hardware and software for semiautomated measurement and analysis protocols could improve 4D CT image quality, patient safety, and efficacy in imaging interpretations (23).

DECT Imaging

Principle

While principles of DECT were described decades ago, the clinical application of DECT in musculoskeletal radiology did not occur until 2006 (24). Current clinical applications for DECT techniques are primarily based on generating two spatially matching CT data sets with two sufficiently different tube energies (eg, 70 and 150 kVp) (25). Some dual-energy techniques are available for single-source CT scanners, such as twin-beam technology and sequential scanning technology (25). Modern dual-source CT scanners acquire the two data sets simultaneously with two pairs of x-ray tubes and corresponding detectors. Single-source CT scanners use rapid voltage switching, energy-resolving detectors, and layer detectors (22,26). Acquiring the two data sets with different tube energies sequentially (eg, in head-to-foot and foot-to-head direction) is practical for older generations of CT scanners without the ability to recognize patient motion.

Clinical Utility

Many postprocessing algorithms are available for DECT, but in clinical musculoskeletal radiology the algorithms most commonly used include the reduction of orthopedic implant-induced metallic streak artifacts (27), monosodium urate crystal detection and quantification in tophaceous gout (28), bone marrow edema maps (29), and the highlighting of collagen-rich tissues such as intervertebral disks (30).

DECT-based monoenergetic data sets between 130 and 190 keV reduce metallic implant-induced bright streak artifacts, thereby reducing the obscuration of the underlying bone and soft tissue and improving assessments of subjects such as bone-implant fixation, fracture healing, and neoplasms (31). Combining the virtual monoenergetic images, projection-based metal artifact reduction, like iterative metal artifact reduction, is also useful. Previously, combining virtual monoenergetic images and iterative metal artifact reduction has been reported to be the most effective method to reduce metallic artifacts and bright and dark streaks (27).

DECT also provides a tool for the noninvasive diagnosis of gout by differentiating and quantifying calcium phosphate and monosodium urate deposits (28). Results from a 2018 systematic review and meta-analysis (32) showed that the pooled sensitivity and specificity of DECT in the diagnosis of gout was 88% and 90%, respectively; however, DECT may have lower accuracy in the detection of early-stage and non-tophaceous gout (33). A phantom study demonstrated that DECT had low accuracy for differentiating calcium pyrophosphate from calcium hydroxyapatite crystals (34). It should be noted that accuracy is influenced by the density of materials being imaged, as it is difficult to separate inadequately dense materials with DECT (35).

Radiography and CT have limited diagnostic performance in the detection of nondisplaced fractures and their associated bone marrow edema, which has been the domain of MRI (36). However, DECT-based virtual noncontrast techniques can be used to create bone marrow edema maps that indicate osseous stress reaction and nondisplaced fractures. The quality of these maps approaches that of images obtained from MRI, which may eliminate the need for confirmatory MRI in emergency situations (Fig 2), increasing the diagnostic performance in the detection of and differentiation between acute from nonacute fractures in the vertebral bodies (37) and appendicular bones (38). DECT can also help detect inflammatory sacroiliitis in spondyloarthropathy (39) and bone marrow infiltration in patients with suspected multiple myeloma and monoclonal gammopathy with high accuracy (40). However, to attain a high level of specificity, certain technical factors must be considered, such as employing the dual-source technique, using both bone and soft-tissue kernels, and having the evaluation performed by experienced readers (37).

DECT differentiation of collagen-rich soft tissues from bone and other soft tissues permits color-coded highlighting of intervertebral disks and tendons to improve the visualization of abnormalities. Compared with gray-scale CT, DECT-based color-coding of intervertebral disks improved the sensitivity and specificity for diagnosing lumbar disk herniations from 80% to 91% and from 85% to 92%, respectively (Fig 3) (30).

Advantages and Disadvantages

DECT is particularly suited for metal artifact reduction and is more capable than MDCT in the characterization of tissue material composition in certain pathologies where tissue density is altered (eg, tophaceous gout). However, unfamiliarity with DECT limits its utility as a routine diagnostic modality in clinical practice with adequate inter- and intraobserver agreement.

Future Directions

While DECT has established its role as a diagnostic tool for trauma, rheumatologic, gout, and neoplasm imaging, existing data on its diagnostic accuracy may have generalizability restrictions. In most studies, DECT images were interpreted by board-certified, experienced radiologists, which may have resulted in higher sensitivity and/or specificity. Therefore, more studies involving less experienced readers are warranted (41). DECT has mostly been used to diagnose traumatic bone marrow edema. Thus, future research concentrating on the detection of nontraumatic bone marrow edema, such as infection, bone tumors, avascular necrosis, and stress fracture, will be valuable (42).

Nonetheless, there are certain limitations for DECT use in an acute setting, which could be investigated in future studies. The first limitation pertains to the interference of the adjacent cortex's spatial averaging effects with the visualization of bone marrow edema near the cortical bone. Consequently, bone marrow edema that is traumatic and restricted to the area beneath the cortex might be overlooked. In addition, bone marrow edema detection could be influenced by various factors, including bone marrow abnormalities and tumor infiltration, bone marrow composition (eg, such as cases involving physiologic red marrow in younger individuals), and bone marrow reconversion (43).

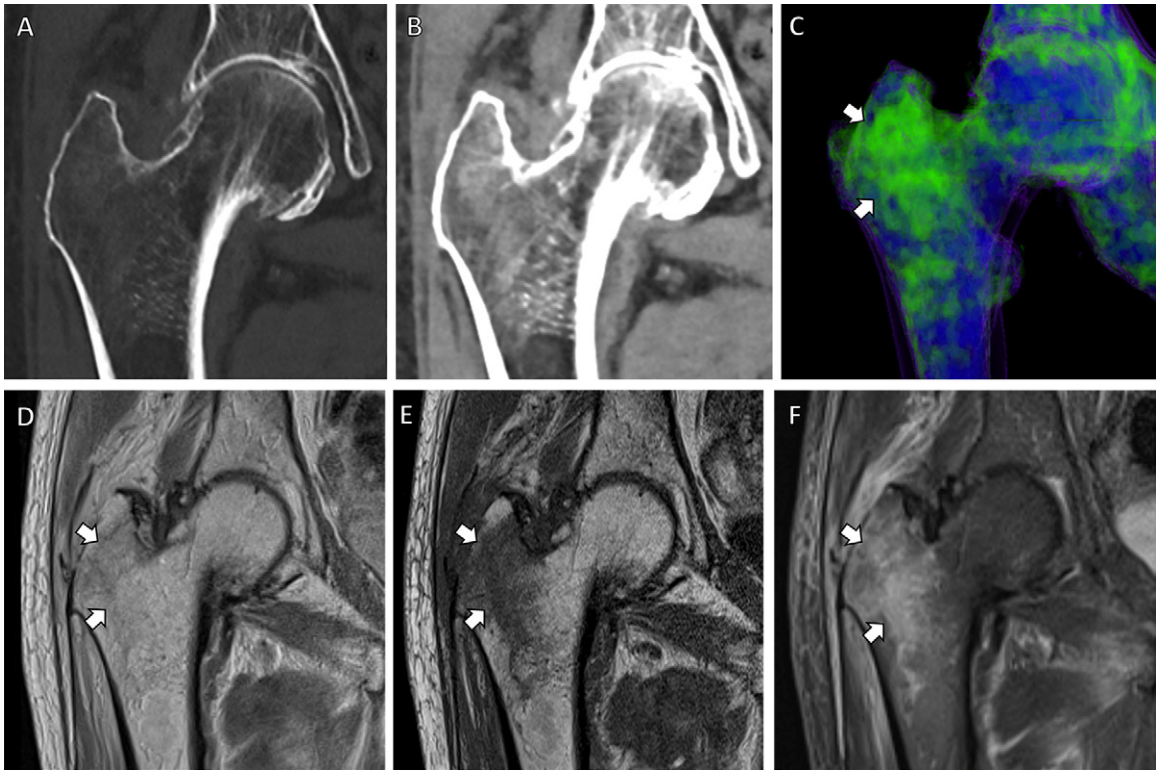

Figure 2: Dual-energy CT–based virtual noncontrast coronal images in an 83-year-old male patient with right-sided hip pain. **(A, B)** CT scans obtained with bone **(A)** and soft-tissue **(B)** windows show bone marrow edema in the right greater trochanter. **(C)** Bone marrow edema map redemonstrates these findings in precise detail (arrows). Corresponding **(D)** coronal proton density, **(E)** coronal T1-weighted, and **(F)** coronal T2-weighted fat-suppressed MRI scans demonstrate a nondisplaced microtrabecular fracture (arrows) in the same region.

CBCT Imaging

Principle

First available in the 1990s (44), CBCT systems use large-area (up to 43 × 43 cm^2) digital flat-panel detectors to obtain 3D images in a single gantry rotation. Compared with conventional MDCT detectors, the advantages of flat-panel detectors include smaller (approximately 150 μm) and isotropic (no difference between the in-plane and section directions) pixels, lower weight and more compact dimensions of the CT scanner device, lower radiation dose, and generally lower cost per examination. Owing to these features, flat-panel detectors enabled the development of tomographic devices for various point-of-care applications where the use of MDCT was limited either because of cost and patient access (eg, dental radiology) or logistics (eg, interventional guidance in surgery and radiation therapy).

Clinical Utility

A variety of scanners for dedicated diagnostic extremity CBCT are now available, enabling either bilateral or unilateral weight-bearing acquisitions. The scan range of these devices is limited to the foot, ankle, and knee, but some more recently developed machines have expanded this range to include the hip. Ongoing research efforts aim to identify quantitative anatomic measurements sensitive to weight bearing that could aid in the assessment of such things as syndesmotic injuries (45) and internal derangements (eg, meniscal extrusion) (Fig 4) (46,47). Translation of such measurements into reliable diagnostic markers will require demonstrating their reliability, protocol standardization, and testing their feasibility in large-scale clinical studies. For instance, in a study performed to assess the reliability and reproducibility of syndesmosis measurements using weight-bearing CBCT images and compare them with non–weight-bearing measurements (45), two CBCT examinations of the symptomatic ankle—one non–weight-bearing and one weight-bearing—were performed. Different categories of measurements were evaluated, and intra- and interobserver correlation and correlation for these measurements obtained between weight-bearing and non–weight-bearing images were analyzed. The results indicated that syndesmotic measurements under weight-bearing conditions are feasible and reproducible, with a high level of agreement among observers (45).

The utility of CBCT in musculoskeletal imaging extends beyond weight-bearing imaging. For example, CBCT typically exhibits better spatial resolution than conventional MDCT, and, importantly, CBCT resolution is generally consistent in all viewing planes (ie, isotropic). Therefore, this method is particularly well-suited for evaluating fine, high-contrast structures such as subchondral bone trabecular architecture (Fig 5). This capability could be especially useful for certain clinical applications, such as fracture

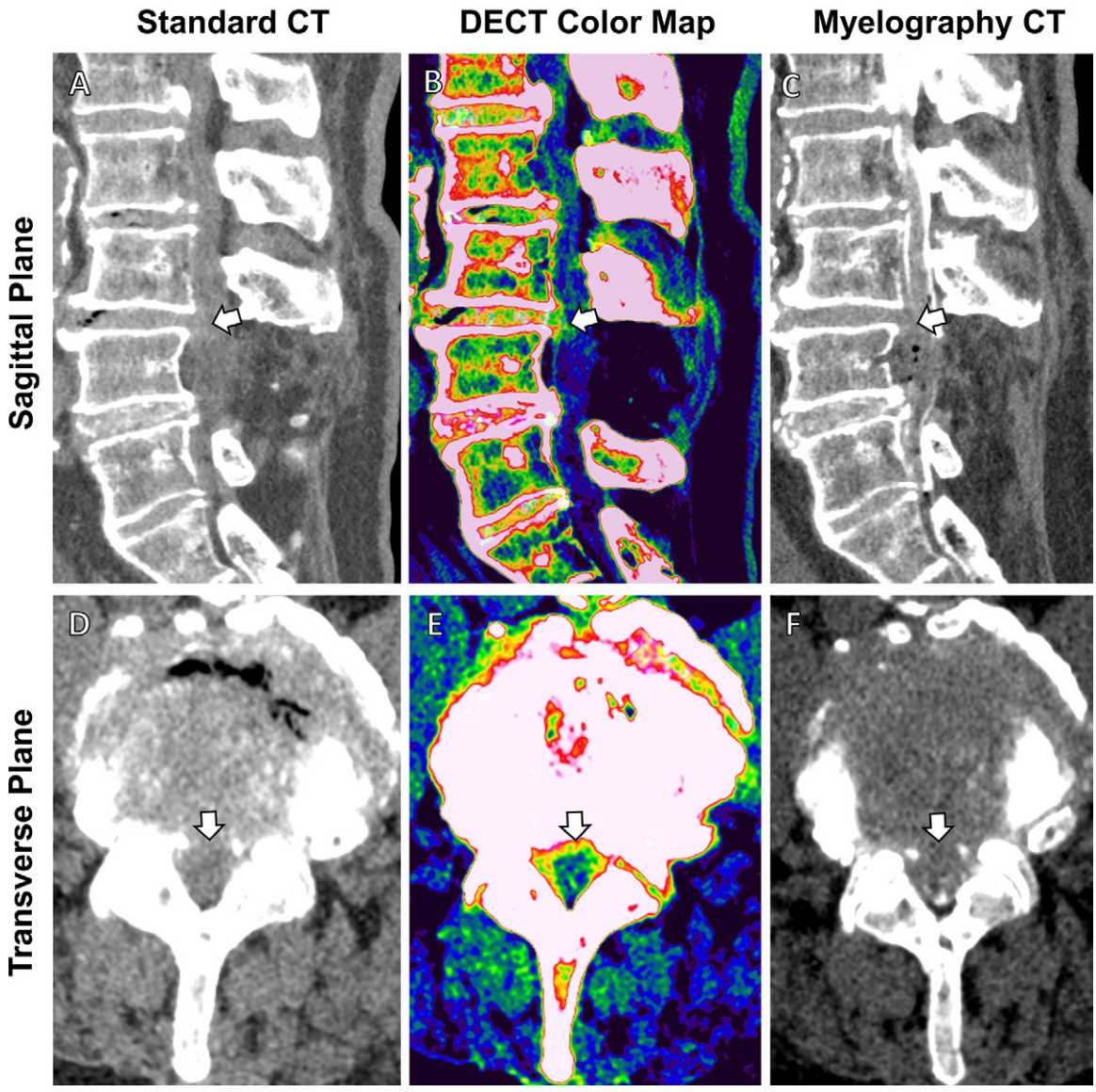

Figure 3: Comparison of standard CT, dual-energy CT (DECT)–based color-coding, and myelography CT in a 78-year-old woman with recurring back pain after L4 decompression surgery. **(A, D)** Sagittal and transverse images from standard CT are suggestive of intervertebral disk protrusion at the L3-L4 level (arrow). **(B, E)** These findings are confirmed in higher detail (arrow) on **(B, E)** axial and sagittal color map images from DECT (green indicates annulus fibrosis, nucleus pulposus, and spongy bone and/or marrow; red and salmon indicate the compact bone; and blue indicates other ligamentous tissue) and **(C, F)** myelography CT scans.

detection and healing assessment. Indeed, CBCT was shown to be more reliable than radiography (48) and shows very strong agreement with MDCT in these settings while reducing the mean CT dose index value by more than 75% (49). It has also been demonstrated that delayed CBCT with intra-articular contrast material has the potential for quantitative imaging of the knee joint, articular cartilage injuries, and subchondral bone changes due to improved contrast resolution from intraarticular contrast material and inherently increased spatial resolution of CBCT compared with conventional MDCT for the assessment of delicate intraarticular structures (50).

Surgical guidance is another area where CBCT is being increasingly used. Here, the ability to develop relatively light-weight and compact tomographic devices is particularly beneficial because of space and logistical constraints. Intraoperative CBCT devices range from C-arms (ceiling-mounted or mobile) with 3D imaging capability (in addition to fluoroscopy) to specialized scanners developed specifically for intraoperative use (eg, the *O*-arm system from Medtronic, which features a breakable gantry for ease of access). The advantages of CBCT in navigation and the assessment of surgical outcomes have been shown in pedicle screw placement in spine surgery (51), displaced acetabular fractures (52), and syndesmotic injuries (53). In addition to these uses, CBCT devices with large-bore diameters have been used in 3D stitching, a process in which a composite 3D image is reconstructed using multiple smaller images

(54). Although primarily used in maxillofacial imaging, the accuracy of 3D stitching suggests that it maybe be a useful for CBCT technology in broader musculoskeletal imaging applications (55).

Considering the relatively slow scanning time of CBCT systems (typically >10 seconds with the latest generation flat-panel detectors), the development of postprocessing algorithms for motion correction is an area of great interest. For example, a 3D autofocus algorithm that reduces artifacts by estimating patient motion significantly improved the readability of lower-extremity CBCT scans as assessed with visual grading characteristics.

Advantages and Disadvantages

Compared with conventional MDCT, CBCT is particularly distinct because of the feasibility of weight-bearing imaging. In addition, compared with MDCT, CBCT can be easily installed in the clinical area due to its smaller size and decreases the radiation dose for various peripheral joint diagnostic tasks, such as fracture detection and healing assessment. The primary disadvantage of CBCT involves limited contrast resolution, which hinders its ability to help assess soft tissues compared with conventional MDCT.

Future Directions

In the future, advances in musculoskeletal CBCT are likely to involve implementing spectral (ie, photon-counting) imaging techniques to use the increased spatial and contrast resolution associated with these techniques; CBCT platforms using PCCT for small-animal imaging have already been developed (56). While large-area PCDs in a format similar to flat-panel detectors are not yet available, the recent introduction of dual- and multilayer flat-panel detectors (57) has made single-scan dual-energy CBCT feasible. Coupled with advanced artifact correction techniques (including scatter correction), dual-energy techniques may enable improved contrast delineation in arthrography and, potentially, quantitative assessment of bone composition, including bone marrow edema (58).

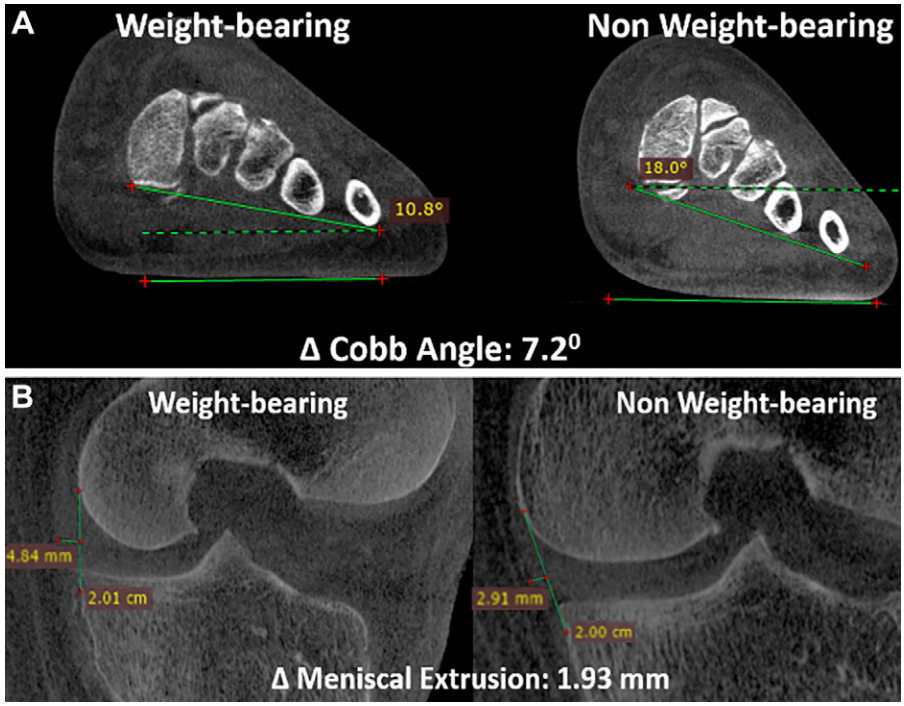

Figure 4: **(A)** Sagittal cone-beam CT (CBCT) images in a 31-year-old male patient with a 6-month history of dorsal midfoot pain. CBCT can be used to show differences in weight-bearing and non–weight-bearing states. In this example, it accurately shows reduction in coronal forefoot arch angle. **(B)** Sagittal CBCT images in a 55-year-old male patient with chronic knee pain. Weight-bearing CBCT and non–weight-bearing CBCT can also be used to measure enhanced meniscal extrusion during physiologic weight-bearing loads (1.3 mm change).

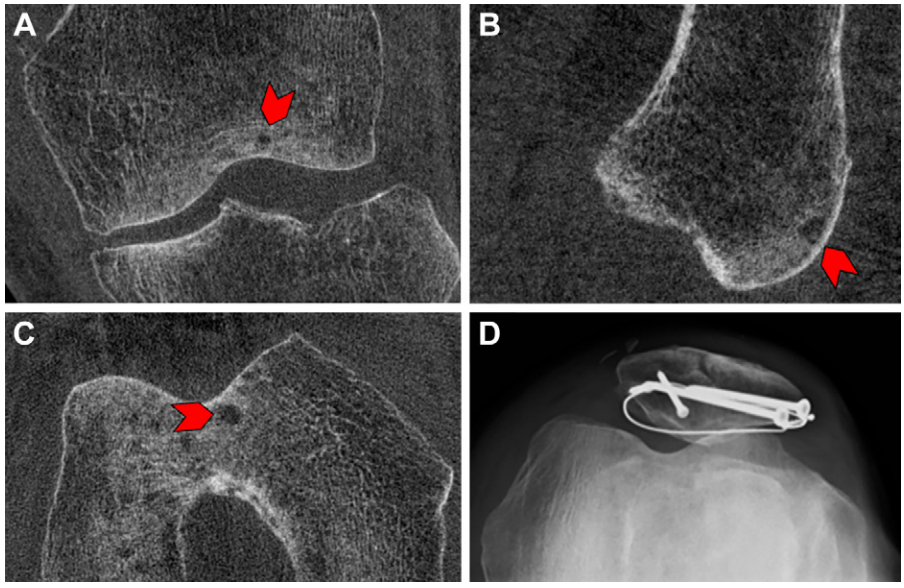

Figure 5: Images in a 68-year-old male patient 9 months after open reduction and internal fixation for a patellar fracture. Cone-beam CT scans in the **(A)** coronal, **(B)** sagittal, and **(C)** axial planes show a small subchondral cyst (arrowhead). **(D)** Skyline view radiograph of the same knee demonstrates the hardware used for open reduction and internal fixation; however, no subchondral cyst is detectable on the radiograph.

The range of applications of weight-bearing CBCT could also be expanded beyond the extremities. Recently, upright CBCT of the spine has been demonstrated using a twin-robotic x-ray system, where the source and the flat-panel detector are moved by independently operated

ceiling-mounted mechanical arms (59). Initial studies on this device indicated potential applications in 3D assessment of spine stability with CBCT under weight-bearing flexion and extension and the ability to quantify neuroforaminal stenosis in the upright body position (60). In addition to weight-bearing imaging, the flexibility of imaging trajectory design provided by the emerging robotic x-ray systems will likely benefit other areas of musculoskeletal radiology. Examples include reduced artifacts due to shoulders in CBCT of the cervical spine using tilted scan orbits (61) and optimizing system magnification for high-resolution assessment of the extremities (62). Furthermore, because these devices are gantry-free, they permit tomographic examinations in settings where patient positioning might be challenging in conventional MDCT—for example, in imaging of acute elbow trauma, where twin-robotic CBCT yielded similar or better sensitivity compared with traditional radiography (63).

Furthermore, the limitations of CBCT, such as susceptibility to motion artifacts in patients with tremors or in children, restricted field of view, and limited ability to evaluate soft-tissue pathology, may warrant further investigation in future studies (64).

High-Resolution Peripheral Quantitative CT

Principle and Clinical Utility

High-resolution peripheral quantitative CT, first introduced in 2005, is a low-dose imaging modality commonly used to access both bone microarchitecture and volumetric bone mineral density (65). The isotropic voxel size of high-resolution peripheral quantitative CT devices is typically either 82 or 61 μm (66,67). Similar to CBCT, it was founded based on cone-beam technology and can generate 3D volume and surface reconstruction (66). The effective radiation dose of high-resolution peripheral quantitative CT is also low, at a value of 3–5 μSv for a scan of the distal radius or tibia (65).

Advantages and Disadvantages

Similar to CBCT, advantages of high-resolution peripheral quantitative CT include visualization of bone microarchitecture. High-resolution peripheral quantitative CT is also useful for visualizing and quantifying the peripheral bone microarchitecture, but its utility for soft-tissue tasks remains limited.

Future Directions

Ongoing research into applications of high-resolution peripheral quantitative CT has included expanded applications of high-resolution peripheral quantitative CT technology for soft-tissue visualization tasks (68). In addition, machine learning applications could have a role in the use of high-resolution peripheral quantitative CT images (69). To further expand the usage of high-resolution peripheral quantitative CT, additional studies into the accuracy and diagnostic utility of the modality to imaging of nonosseous tissue is warranted.

High-Spatial-Resolution CT

Principle and Clinical Utility

High-spatial-resolution CT is a recently emerged multidetector CT technology characterized by an x-ray detector with a pixel size of 250 μm, which can aid visualization of high-resolution details in musculoskeletal CT (70). High-spatial-resolution CT images have been able to depict high-contrast trabecular bone details as small as 150 μm (71) and may double the in-plane spatial resolution compared with MDCT systems. However, this comes at the cost of an approximately 23% increase in radiation dose (70). Using human bone samples, improved visualization and reduced error in quantification of trabecular bone microarchitecture (ie, trabecular thickness, spacing, and bone volume fraction) was observed using high-spatial-resolution CT compared with conventional MDCT (71).

Advantages and Disadvantages

High-spatial-resolution CT allows for increased contrast and spatial resolution for the detailed assessment and quantification of trabecular bone microarchitecture of the axial skeleton (eg, spine) at a tradeoff of increased radiation exposure.

Future Directions

Ultrahigh-resolution body imaging is feasible using large-bore high-spatial-resolution CT and can provide a simultaneous robust quantitative assessment of bone density and spine degeneration during chest or abdominal CT in various medical conditions. Future research to identify and assess the predictive value of high-spatial-resolution CT–derived markers for axial bone trabecular microarchitecture are warranted and could be carried out in patients with maladies that require body CT examinations and for whom there is an increased risk of progressive osteoporosis.

Deep learning–based image reconstruction algorithms, which have the potential to reduce the radiation required to achieve optimal spatial resolution for high-spatial-resolution CT, are not adequately evaluated in the existing literature. In addition, the clinical impact of high-spatial-resolution CT has not been comprehensively evaluated as of yet. Given the size of the used phantom, the majority of the relevant research is pertinent to peripheral joints; additional research is required to evaluate the effect of the assessed factors on central joints. Despite the potential advantages of achieving optimal spatial resolution, moderate to high dose levels are still required, and additional research is required to evaluate the risk-to-benefit ratio of these dose requirements in clinical settings.

PCCT Imaging

Principle

In 2021, the first PCCT system was approved for clinical use in the United States. This marked a major advancement in CT imaging technology. PCDs not only measure x-ray projections with less noise and improved spatial resolution as

compared with EIDs, but they also retain tissue-specific information of the body by means of x-ray spectra, thus providing improved contrast resolution for bone and soft-tissue diagnostic tasks. There are inherent limitations to optimizing image quality using current EID CT detectors; they all measure the intensity of x-rays by first converting x-ray photons via a scintillating step into visible light, the aggregate of which is then transformed into electronic charges, and, finally, digital data (Fig 6A). This series of conversions introduces electronic noise into the x-ray data used for image creation, and spectral information about each x-ray photon is lost. The optical reflectors used in EIDs do not detect x-rays, but rather create dead spaces in the array and therefore decrease the geometrical efficiency (Fig 7). Using smaller pixels, the geometrical efficiency drops further (hence, the dose efficiency degrades). This restricts the minimum size of detector pixels, constraining pixel sizes to a lower limit of 0.25–0.63 mm. In contrast, a PCD directly converts each x-ray photon energy into an electronic charge cloud, which creates a pulse at the corresponding anode (Fig 6B). The height of the pulse is proportional to the incident photon energy, and an electronic circuitry (of PCD) detects and counts an event when the pulse exceeds a preset threshold energy. After each projection, which lasts approximately 200 μsec, the number of counted events is read out from the PCD. PCDs typically have two to six energy thresholds set at different energies. The PCD acquires information about the x-ray energy spectrum, which can be directly translated to improved contrast resolution of PCD CT examinations. Unlike EIDs, PCDs do not require optical reflectors and, as a result, have excellent geometric efficiency. In addition, without fixed reflector sizes, smaller detector pixels can be designed to achieve high spatial resolution, as low as 0.125 mm, without the constraints of geometric dose efficiency (Fig 7) (72).

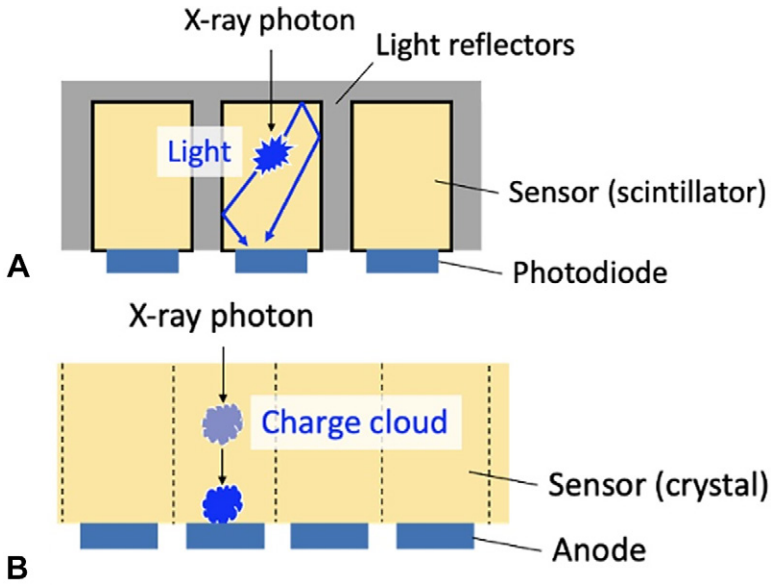

Figure 6: Diagrams show side views of **(A)** current energy-integrating CT detectors and **(B)** photon-counting detectors. **(A)** Multiple detector segments separate the scintillators. When an x-ray photon enters a scintillator, light is generated, which is subsequently converted to an electrical signal by the photodiode. **(B)** When x-ray photons enter the crystal detector, a charge cloud is generated, which is attracted to the anode by an electrical field and generates a pulse. Spatial resolution is inversely related to the anode size.

The material information acquired with PCDs allows for improved contrast resolution and improved quantitative and material-specific imaging (Fig 8). Quantitative images acquired using PCCT are free from beam hardening (shading and/or streaking) artifacts and monoenergetic CT data. Material-specific imaging includes iodine maps, fat fractions, bone images, iron density maps, virtual noncalcium images to depict bone edema, virtual non–contrast-enhanced CT images, and K-edge imaging with novel contrast media, including gold or bismuth (73). PCCT counts each photon individually, irrespective of the measured photon energy. Consequently, the low-energy photons contribute more to the image contrast in PCCT, enhancing the image contrast and contrast-to-noise ratio of iodine-based contrast material. Spectral PCCT scanners measure incident photon energy to identify contrast agents based on their x-ray attenuation characteristics, a technique called K-edge imaging. Gold, bismuth, and ytterbium nanoparticles are potential contrast agents for spectral PCCT imaging. Gold nanoparticles are also used as radiation therapy adjuvants and photothermal ablation adjuvants (73,74). As it may be challenging for humans to parse through the large amount of data provided by PCCT, artificial intelligence will likely play an important role in identifying valuable clinical information buried in the spectral data. This information could then be used to build risk prediction models that could aid in the diagnosis and/or treatment of musculoskeletal ailments.

Clinical Utility

The higher-quality data obtained at PCCT results in improved spatial resolution, enabling discernment of small structures such as cortical and trabecular architecture (Figs 9, 10). One prospective study using a clinical PCD system to evaluate the wrists of 12 individuals with CT-indicating conditions including degenerative arthritis and fracture found that, compared with EID scans, PCCT images enabled better visualization of osseous structures and had higher mean Hounsfield units despite a 49% reduction in the acquisition radiation dose (75). Similar results were reported in a study of four human cadaveric wrist specimens performed with PCCT using radiation doses either equal to or 50% less than those used for EID CT (76). The investigators found that images obtained with PCCT had a 59% lower contrast-to-noise ratio, a 66% higher trabecular sharpness, and up to 45% higher cortical sharpness compared with EID CT images, even at half the radiation dose. The value of demonstrating cortical and trabecular anatomy in exquisite detail goes beyond improved visual inspection of bone. For instance, quantitative assessment of bone

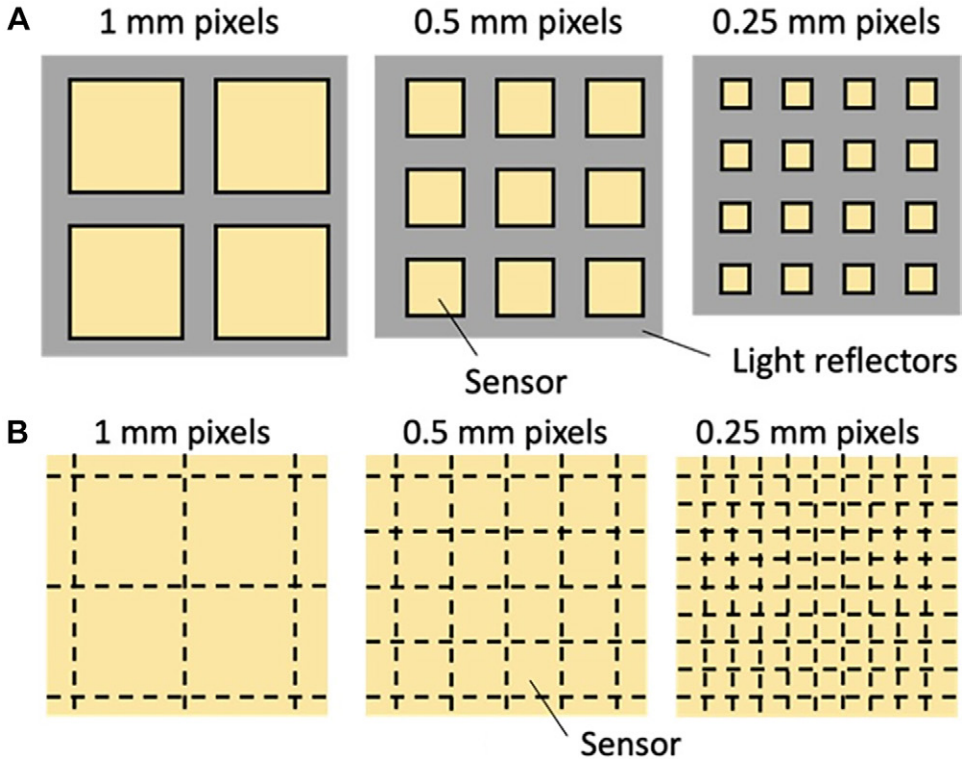

Figure 7: Top views of **(A)** current CT detectors and **(B)** photon-counting detectors (PCDs) with different pixel sizes. **(A)** With reflectors (gray) thickness being fixed, current CT detectors with smaller pixels (yellow squares) have worse geometrical efficiency than detectors with larger pixels due to the increased dead space in between detectors. **(B)** In contrast, because reflectors are not necessary in PCDs, smaller pixel sizes do not accompany larger areas of reflector dead space, effectively rendering 100% geometric efficiencies.

quality related to trabecular spacing and thickness can be extended to central sites such as the spine.

Simultaneous high-resolution imaging with spectral data is feasible with PCDs due to the detectors' ability to help differentiate between individual photons irrespective of the scanning mode. In current musculoskeletal applications of dual-source CT, one chooses between obtaining a high-resolution image to detect subtle fractures or operating the scanner in dual-energy mode to generate virtual noncalcium images that allow visualization of bone marrow edema associated with fractures or intramedullary soft-tissue lesions. PCDs eliminate this trade-off between spatial resolution and multi-energy capabilities. Concurrent high-spatial-resolution imaging with spectral data is also beneficial in the workup of

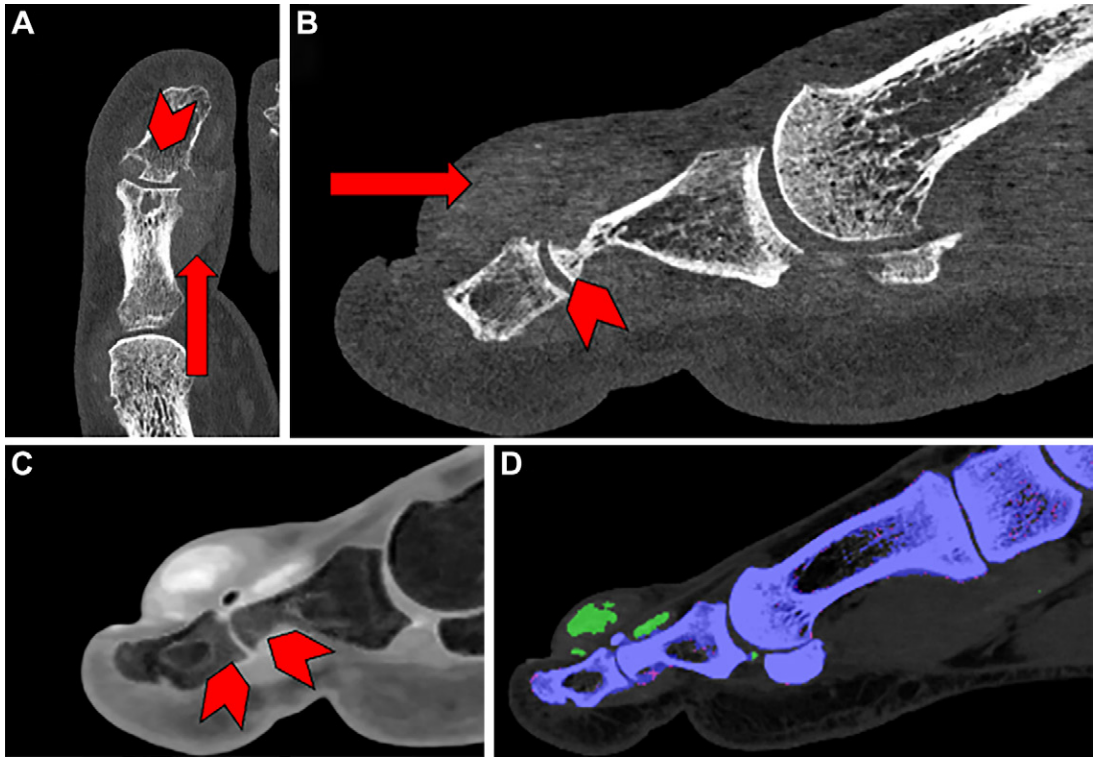

Figure 8: Images in a 58-year-old male patient with pain and swelling of the first digit of the left foot acquired using photon-counting detectors (PCDs). **(A)** Transverse view and **(B)** sagittal view show that periarticular mineralization (arrow) can be seen with associated erosive change (arrowhead). **(C)** Material decomposition acquisition reveals bone edema in the phalanges of the interphalangeal joint (arrowheads). **(D)** Another color-encoded material decomposition image reveals monosodium urate crystal deposits (green).

intraarticular and periarticular pathology with CT arthrography. With one CT acquisition, high-resolution virtual noncontrast images can be generated to develop 3D models, without the need to scan the patient before injection of intraarticular iodinated contrast material.

Higher-energy x-rays have a higher propensity to penetrate metal and have fewer associated artifacts. With PCDs, high energy threshold images can be used to generate images that have decreased metal artifacts and beam hardening. This is crucial for orthopedic imaging in the setting of metallic prosthesis (7). When combined with dedicated x-ray beam shaping techniques, such as tin prefiltration of the x-ray beam, the low-energy photons that are most affected by beam hardening are filtered out of the x-ray spectrum. Finally, virtual monoenergetic images at high effective energies can be used to mitigate the effect of metal artifacts. A study comparing clinically indicated PCCT of the spine in patients with metallic implants showed significant improvements in image quality, noise, and diagnostic confidence when comparing PCCT at 130 keV to PCCT at 65 keV (77). Importantly, all of these reconstruction techniques are compatible with commercially available projection-based metal artifact reduction algorithms.

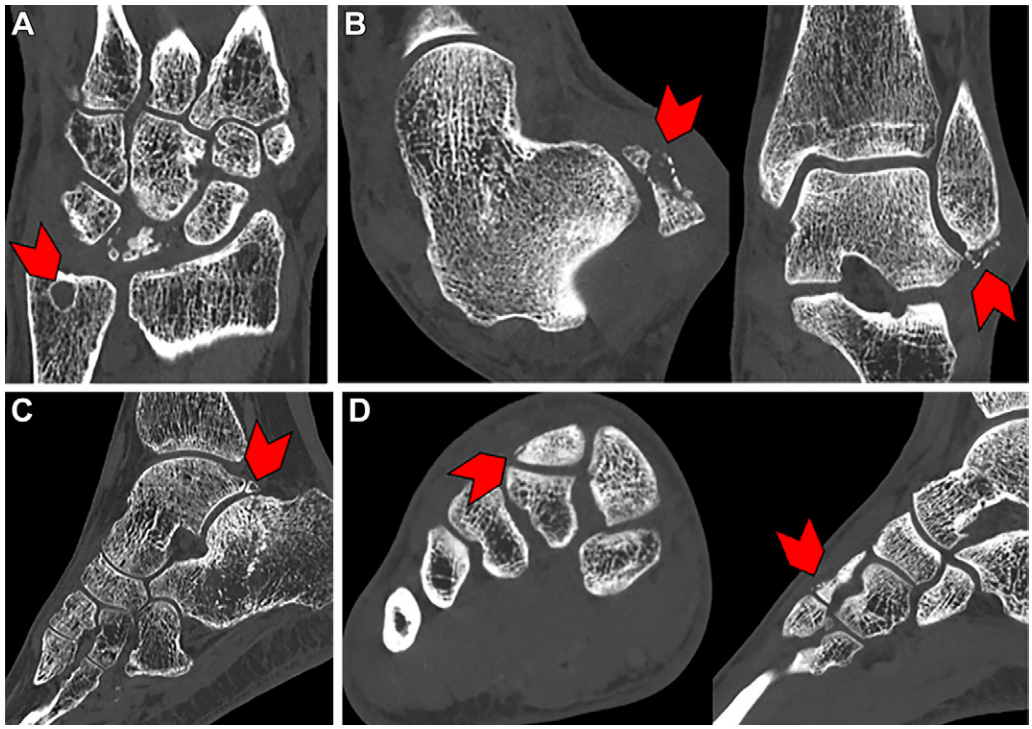

Figure 9: Example photon-counting CT images in patients with various pathologies. **(A)** Coronal image in a 47-year-old female patient with Kienböck disease. Cystic abnormality can be seen at the fovea of the ulna (arrowhead). **(B)** Coronal and axial images in a 55-year-old female patient with lateral malleolus fracture. Punctate foci at the tip of the lateral malleolus of the distal fibula (arrowheads) indicate a subacute avulsion fracture. **(C)** Sagittal image in a 74-year-old male patient with a comminuted transverse fracture of the calcanea body with surrounding patch sclerosis (arrowhead). **(D)** Sagittal and coronal images in a 17-year-old male patient with dorsal foot pain. A small fracture is seen along the dorsal aspect of the middle cuneiform at the second tarsometatarsal joint (arrowheads).

Finally, most musculoskeletal CT imaging practices use low radiation dose scanning protocols; however, this leads to more pronounced electronic noise. Alternatively, PCCT techniques use low-energy threshold photons, which are associated with electronic noise but can be excluded from the CT image at the time of reconstruction, thus allowing for better image quality.

Advantages and Disadvantages

The main advantages of PCCT are markedly enhanced spatial and contrast resolution as compared with MDCT despite the reduction in radiation exposure. Such a tremendous advantage suggests a prominent role of PCCT for most musculoskeletal imaging applications, replacing conventional MDCT in the future. The cost and availability of PCCT detectors remain a challenge for the immediate adoption of PCCT technology.

Future Directions

The markedly improved contrast resolution and high-resolution data obtained with PCCT represent as major advancement for both bone and soft- tissue CT diagnostic tasks. Further studies are necessary to compare the performance of PCCT versus EID CT for diagnosing different musculoskeletal pathologies. Such studies could also examine whether diagnostic imaging with PCCT versus EID CT led to differences in patient outcomes and potentially inform the larger-scale adoption of PCD technology.

Novel Postprocessing Techniques

Three-dimensional Printing

Three-dimensional printing technology has been used to generate patient-specific anatomic models for the visualization of and surgical planning for musculoskeletal pathologies. Development of a 3D printed anatomic model typically requires several conversions of CT data from Digital Imaging and Communications in Medicine files, first into a standard triangle language file type and then into a G-code (78). Three-dimensional printers use the G-code as instructions for printing the 3D anatomic structure. These models

have simulated surgical intervention in the preoperative planning for acetabular fractures, and their use has been associated with a reduction in both intraoperative blood loss and operative time (79). Furthermore, 3D printing technology has shown clinical utility in modeling various complex osseous lesions, such as scapular osteochondroma, before surgery (80). Research in this field is rapidly advancing and simultaneously being integrated into clinical practice. For instance, recent optimizations in the 3D printing workflow have reduced the time necessary to print some fracture models by 65% (ie, reduced from 25 hours 26 minutes to 8 hours 40 minutes), allowing easy handling along with lower cost of the 3D printing workflow, making it a viable option for almost any hospital setting (81). This workflow helps improve understanding of the pathology by haptic exploration, planning the fracture reduction strategy, and bending osteosynthesis plates to the anatomy, which can be used as a reduction guide during surgery, saving time and improving implant fit (81). Another area of active research is the prospective application of 3D printing technology for the grafting of bone and cartilage substitutes. Potential tissue-equivalent materials for grafting have already been identified (82).

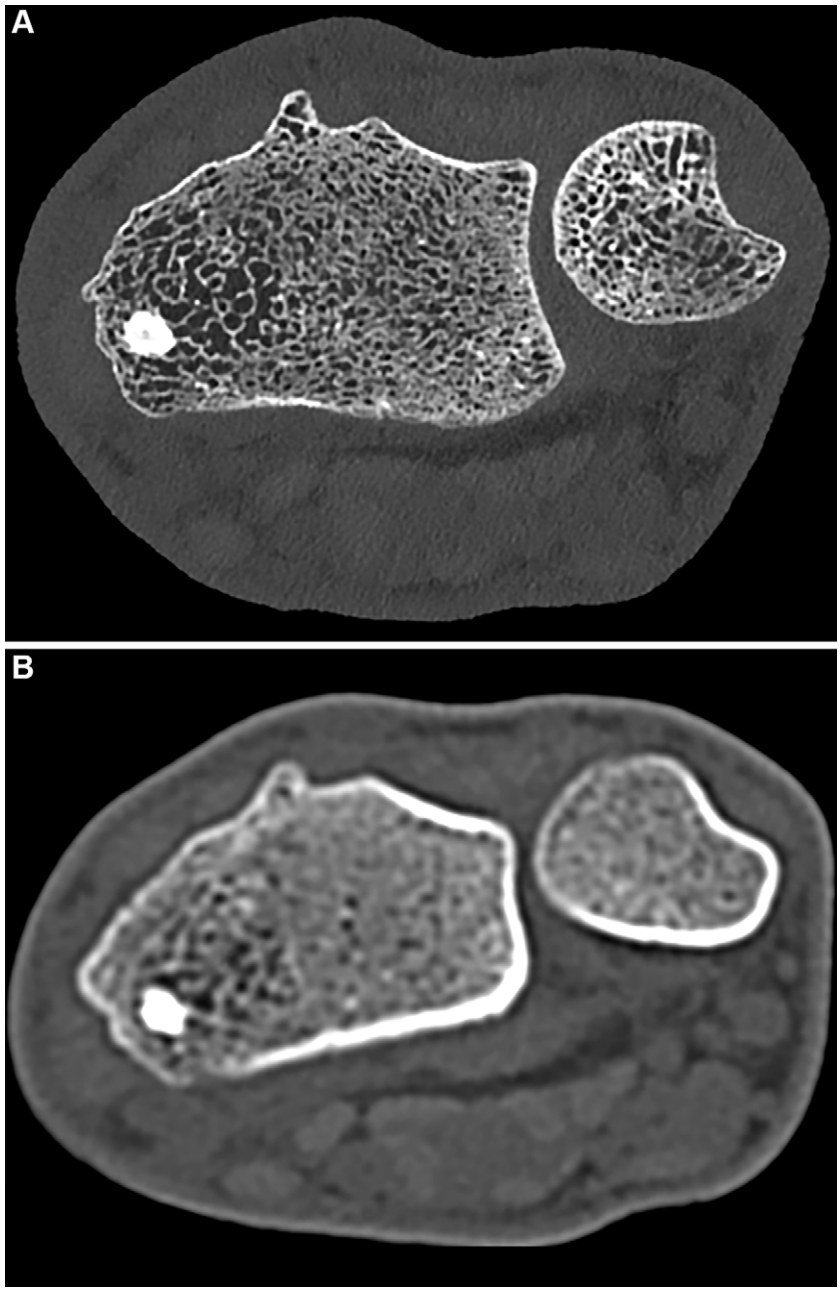

Figure 10: Noncontrast CT images of the distal radius in a 23-year-old male patient. **(A)** Ultrahigh-resolution axial photon-counting CT image (section thickness, 0.2 mm; reconstruction kernel, Br84; 120 kV; volume CT dose index, 12 mGy; window width, 500 HU; window level, 2000 HU) and **(B)** standard-resolution CT scan in the same patient acquired with an energy-integrating detector CT system 5 years earlier (section thickness, 1 mm; reconstruction kernel, B70; 130 kV; volume CT dose index, 15 mGy; window width, 500 HU; window level, 2000 HU; Siemens Emotion 16) show significant difference in visual resolution.

Cinematic Rendering

Cinematic rendering, a postprocessing technique that uses complex light paths and high dynamic range light maps, has enabled more photorealistic CT image reconstruction than contemporary postprocessing techniques such as volume rendering (8). In a study of 16 medical students, participants were able to read and comprehend cinematic rendering–reconstructed musculoskeletal anatomy models faster than conventional volume rendering reconstructions (83). Cinematic rendering reconstructions possess more depth and increased surface detail compared with volume rendering, attributable to cinematic rendering's complex global lighting model (Fig 11) (8). In addition, pictorial essays have highlighted the detail and clarity of cinematic rendering reconstructions in evaluating multifaceted clinical musculoskeletal pathologies, including complex fractures (84). As such, cinematic rendering represents an important innovation in postprocessing CT reconstruction, with both pedagogic and clinical utility in musculoskeletal imaging.

Musculoskeletal CT and Artificial Intelligence

While the application of deep learning to CT examinations has only recently been introduced in a clinical setting, researchers have been studying their ability to automatically detect and characterize musculoskeletal pathologies at CT for decades. Examples of recent advancements include the automated evaluation of traumatic fractures and skeletal metastases (85,86). As a result, along with the growing literature on the development of deep learning–based CT image

processing and analysis, we can anticipate seeing many commercial products implementable on CT examinations performed in routine clinical practice for various musculoskeletal diagnostic tasks.

Conclusion

Recent developments in CT scanner technology, acquisition techniques, and postprocessing methods have made it possible to examine musculoskeletal structures during motion and weight-bearing, as well as to achieve a high spatial resolution for visualization of bone architecture. In addition, novel photon-counting CT techniques have the potential to become more prominent in clinical musculoskeletal imaging due to their higher contrast and spatial resolution and lower radiation exposure compared with conventional CT technologies.

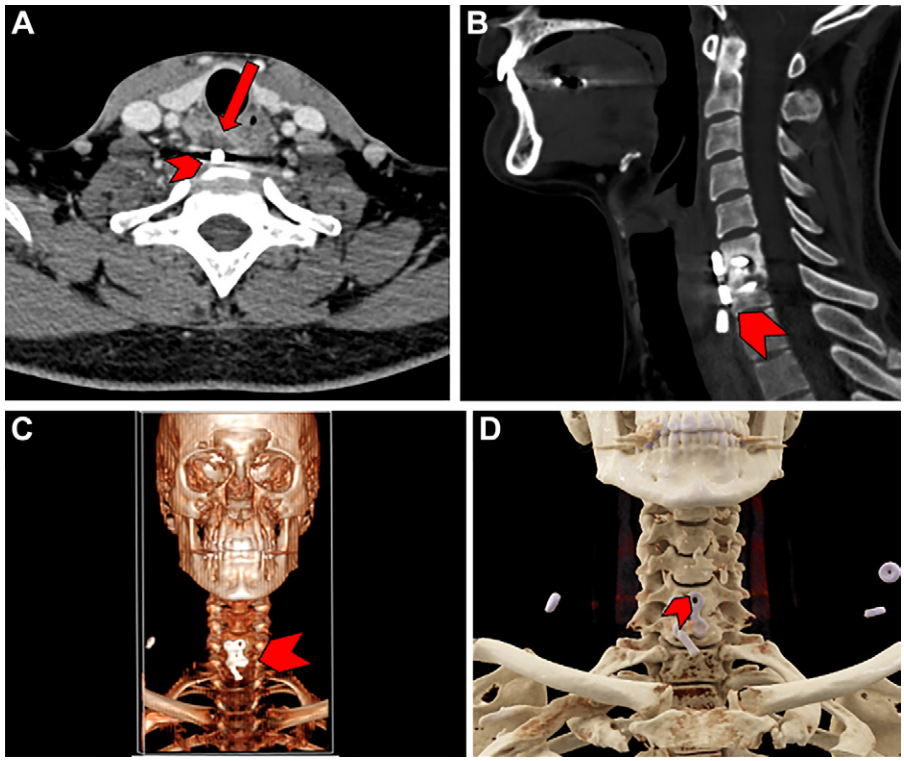

Figure 11: Images in a 30-year-old male patient with a history of anterior cervical discectomy and fusion of the sixth and seventh cervical vertebrae. **(A, B)** Conventional axial **(A)** and sagittal **(B)** CT scans demonstrate the displacement of a screw used for fixation (arrow in **A**). Also demonstrated is an abnormal lucency (arrowhead) indicative of screw loosening or infection. **(C)** Traditional three-dimensional (3D) surface reconstruction demonstrates placement of the implant with moderate resolution (arrowhead). **(D)** Cinematic rendering of the acquired CT scan clearly demonstrates the screw (arrowhead) and hardware plate used in the anterior cervical discectomy and fusion surgery. Such rendering can help those without extensive radiologic experience to interpret scans in an intuitive manner and resembles real anatomic structures more accurately than traditional 3D surface reconstruction.

Disclosures of conflicts of interest: S.D. No relevant relationships. **F.I.B.** No relevant relationships. **J.G.K.** No relevant relationships. **E.G.** No relevant relationships. **H.A.I.** No relevant relationships. **K.M.** No relevant relationships. **K.T.** Payments to the institution from Siemens Healthineers; grants to the institution from Canon Medical Systems; consulting fees from Suzhou Bowing Medical; payment or honoraria for lectures, presentations, speakers bureaus, manuscript writing, or educational events from University of Seoul, Yale University, Japan Radiological Congress, and Taylor & Francis CRC Press; International Patent Application Number Pct/US2021/015288 filed on January 27, 2021 and published as WO 2021/154851A1 on August 5, 2021. **J.F.** Member of *Radiology* editorial board, grants or contracts from GE Healthcare, Siemens, QED, and SyntheticMR; consulting fees from Siemens, GE Healthcare, Boston Scientific, Mirata Pharma, and Guerbet; patents planned, issued or pending with Siemens Healthcare, Johns Hopkins University, and New York University; participation on a DataSafety Monitoring Board or Advisory Board at Siemens, SyntheticMR, GE Healthcare, QED, BTG, ImageBiopsy Lab, Boston Scientific, Mirata Pharma, and Guerbet. **J.A.C.** No relevant relationships. **A.G.** Consulting fees from Pfizer, Coval, TrialSpark, ICM, Novartis, and TissueGene; stock or stock options in BICL, LLC; consultant to the editor of *Radiology*. **E.K.F.** No relevant relationships. **W.B.Z.** Research grants from Carestream Health, Siemens Healthineers, and Canon Medical, and NIH (R01-EB-018896, R01-EB-029446, and R01-EB-025470); Dual-Energy Cone-Beam Computed Tomography with a Multiple-Source, Single-Detector Configuration, U.S. Patent US10631800B2; System and Method For Artifact Reduction In An Image, U.S. Patent 20220028131.

References

1. Hess EP, Haas LR, Shah ND, Stroebel RJ, Denham CR, Swensen SJ. Trends in computed tomography utilization rates: a longitudinal practice-based study. J Patient Saf 2014;10(1):52–58.
2. Mettler FA Jr, Thomadsen BR, Bhargavan M, et al. Medical radiation exposure in the U.S. in 2006: preliminary results. Health Phys 2008;95(5):502–507.
3. Brink JA, Heiken JP, Wang G, McEnery KW, Schlueter FJ, Vannier MW. Helical CT: principles and technical considerations. RadioGraphics 1994;14(4):887–893.
4. Halpenny D, Courtney K, Torreggiani WC. Dynamic four-dimensional 320 section CT and carpal bone injury - a description of a novel technique to diagnose scapholunate instability. Clin Radiol 2012;67(2):185–187.
5. Marin D, Boll DT, Mileto A, Nelson RC. State of the art: dual-energy CT of the abdomen. Radiology 2014;271(2):327–342.
6. Carrino JA, Al Muhit A, Zbijewski W, et al. Dedicated cone-beam CT system for extremity imaging. Radiology 2014;270(3):816–824.
7. Baffour FI, Glazebrook KN, Ferrero A, et al. Photon-Counting Detector CT for Musculoskeletal Imaging: A Clinical Perspective. AJR Am J Roentgenol 2023;220(4):551–560.
8. Dappa E, Higashigaito K, Fornaro J, Leschka S, Wildermuth S, Alkadhi H. Cinematic rendering - an alternative to volume rendering for 3D computed tomography imaging. Insights Imaging 2016;7(6):849–856.
9. Wollschlaeger LM, Boos J, Jungbluth P, et al. Is CT-based cinematic rendering superior to volume rendering technique in the preoperative evaluation of multifragmentary intraarticular lower extremity fractures? Eur J Radiol 2020;126:108911.
10. Hugo GD, Rosu M. Advances in 4D radiation therapy for managing respiration: part I - 4D imaging. Z Med Phys 2012;22(4):258–271.
11. Demehri S, Wadhwa V, Thawait GK, et al. Dynamic evaluation of pisotriquetral instability using 4-dimensional computed tomography. J Comput Assist Tomogr 2014;38(4):507–512.
12. Demehri S, Chalian M, Farahani SJ, Fishman EK, Fayad LM. Detection and characterization of tendon abnormalities with multidetector computed tomography. J Comput Assist Tomogr 2014;38(2):299–307.
13. Haj-Mirzaian A, Thawait GK, Tanaka MJ, Demehri S. Diagnosis and Characterization of Patellofemoral Instability: Review of Available Imaging Modalities. Sports Med Arthrosc Rev 2017;25(2):64–71.
14. Gobbi RG, Demange MK, de Ávila LFR, et al. Patellar tracking after isolated medial patellofemoral ligament reconstruction: dynamic evaluation using computed tomography. Knee Surg Sports Traumatol Arthrosc 2017;25(10):3197–3205.
15. Mousavian A, Shakoor D, Hafezi-Nejad N, et al. Tibiofibular syndesmosis in asymptomatic ankles: initial kinematic analysis using four-dimensional CT. Clin Radiol 2019;74(7):571.e1–571.e8.

16. Gondim Teixeira PA, Formery A-S, Jacquot A, et al. Quantitative Analysis of Subtalar Joint Motion With 4D CT: Proof of Concept With Cadaveric and Healthy Subject Evaluation. AJR Am J Roentgenol 2017;208(1):150–158.
17. Demehri S, Hafezi-Nejad N, Morelli JN, et al. Scapholunate kinematics of asymptomatic wrists in comparison with symptomatic contralateral wrists using four-dimensional CT examinations: initial clinical experience. Skeletal Radiol 2016;45(4):437–446.
18. Shores JT, Demehri S, Chhabra A. Kinematic "4 Dimensional" CT Imaging in the Assessment of Wrist Biomechanics Before and After Surgical Repair. Eplasty 2013;13:e9.
19. Goelz L, Kim S, Güthoff C, et al. ACTION trial: a prospective study on diagnostic Accuracy of 4D CT for diagnosing Instable ScaphOlunate DissociatioN. BMC Musculoskelet Disord 2021;22(1):84.
20. Fernquest S, Arnold C, Palmer A, et al. Osseous impingement occurs early in flexion in cam-type femoroacetabular impingement: a 4D CT model. Bone Joint J 2017;99-B(4 Supple B):41–48.
21. Kishida S, Funabashi N, Harada Y, Komuro I, Moriya H. Utility of four-dimensional analysis of the acetabular labrum applying motion-gated multislice computed tomography: comparison with arthroscopy and harris hip score. J Comput Assist Tomogr 2006;30(6):991–1000.
22. Ibad HA, de Cesar Netto C, Shakoor D, et al. Computed Tomography: State-of-the-Art Advancements in Musculoskeletal Imaging. Invest Radiol 2023;58(1):99–110.
23. Wong MT, Wiens C, Kuczynski M, Manske S, Schneider PS. Four-dimensional computed tomography: musculoskeletal applications. Can J Surg 2022;65(3):E388–E393.
24. Mallinson PI, Coupal TM, McLaughlin PD, Nicolaou S, Munk PL, Ouellette HA. Dual-Energy CT for the Musculoskeletal System. Radiology 2016;281(3):690–707.
25. Johnson TRC. Dual-energy CT: general principles. AJR Am J Roentgenol 2012;199(5 Suppl):S3–S8.
26. Ghodasara N, Yi PH, Clark K, Fishman EK, Farshad M, Fritz J. Postoperative Spinal CT: What the Radiologist Needs to Know. RadioGraphics 2019;39(6):1840–1861.
27. Khodarahmi I, Haroun RR, Lee M, et al. Metal Artifact Reduction Computed Tomography of Arthroplasty Implants: Effects of Combined Modeled Iterative Reconstruction and Dual-Energy Virtual Monoenergetic Extrapolation at Higher Photon Energies. Invest Radiol 2018;53(12):728–735.
28. Fritz J, Henes JC, Fuld MK, Fishman EK, Horger MS. Dual-Energy Computed Tomography of the Knee, Ankle, and Foot: Noninvasive Diagnosis of Gout and Quantification of Monosodium Urate in Tendons and Ligaments. Semin Musculoskelet Radiol 2016;20(1):130–136.
29. Zbijewski W, Sisniega A, Stayman JW, et al. Dual-Energy Imaging of Bone Marrow Edema on a Dedicated Multi-Source Cone-Beam CT System for the Extremities. Proc SPIE Int Soc Opt Eng. 2015;9412:94120V.
30. Booz C, Nöske J, Martin SS, et al. Virtual Noncalcium Dual-Energy CT: Detection of Lumbar Disk Herniation in Comparison with Standard Gray-scale CT. Radiology 2019;290(2):446–455.
31. Bamberg F, Dierks A, Nikolaou K, Reiser MF, Becker CR, Johnson TRC. Metal artifact reduction by dual energy computed tomography using monoenergetic extrapolation. Eur Radiol 2011;21(7):1424–1429.
32. Yu Z, Mao T, Xu Y, et al. Diagnostic accuracy of dual-energy CT in gout: a systematic review and meta-analysis. Skeletal Radiol 2018; 47(12):1587–1593.
33. Gamala M, Jacobs JWG, van Laar JM. The diagnostic performance of dual energy CT for diagnosing gout: a systematic literature review and meta-analysis. Rheumatology (Oxford) 2019;58(12):2117–2121.
34. Døssing A, Müller FC, Becce F, Stamp L, Bliddal H, Boesen M. Dual-Energy Computed Tomography for Detection and Characterization of Monosodium Urate, Calcium Pyrophosphate, and Hydroxyapatite: A Phantom Study on Diagnostic Performance. Invest Radiol 2021;56(7):417–424.
35. Christiansen SN, Müller FC, Østergaard M, et al. Dual-energy CT in gout patients: Do all colour-coded lesions actually represent monosodium urate crystals? Arthritis Res Ther 2020;22(1):212.
36. Kijowski R, Fritz J. Emerging Technology in Musculoskeletal MRI and CT. Radiology 2023;306(1):6–19.
37. Ghazi Sherbaf F, Sair HI, Shakoor D, et al. DECT in Detection of Vertebral Fracture-associated Bone Marrow Edema: A Systematic Review and Meta-Analysis with Emphasis on Technical and Imaging Interpretation Parameters. Radiology 2021;300(1):110–119.
38. Booz C, Nöske J, Lenga L, et al. Color-coded virtual non-calcium dual-energy CT for the depiction of bone marrow edema in patients with acute knee trauma: a multireader diagnostic accuracy study. Eur Radiol 2020;30(1):141–150.
39. Wu H, Zhang G, Shi L, et al. Axial Spondyloarthritis: Dual-Energy Virtual Noncalcium CT in the Detection of Bone Marrow Edema in the Sacroiliac Joints. Radiology 2019;290(1):157–164.
40. Kosmala A, Weng AM, Heidemeier A, et al. Multiple Myeloma and Dual-Energy CT: Diagnostic Accuracy of Virtual Noncalcium Technique for Detection of Bone Marrow Infiltration of the Spine and Pelvis. Radiology 2018;286(1):205–213.
41. Wilson MP, Lui K, Nobbee D, et al. Diagnostic accuracy of dual-energy CT for the detection of bone marrow edema in the appendicular skeleton: a systematic review and meta-analysis. Eur Radiol 2021;31(3):1558–1568.
42. Chen Z, Chen Y, Zhang H, Jia X, Zheng X, Zuo T. Diagnostic accuracy of dual-energy computed tomography (DECT) to detect non-traumatic bone marrow edema: A systematic review and meta-analysis. Eur J Radiol 2022;153:110359.
43. Simonetti I, Verde F, Palumbo L, et al. Dual energy computed tomography evaluation of skeletal traumas. Eur J Radiol 2021;134:109456.
44. Spagnuolo G. Cone-Beam Computed Tomography and the Related Scientific Evidence. Applied Sciences (Switzerland). MDPI 2022;12(14):7140.
45. Shakoor D, Osgood GM, Brehler M, et al. Cone-beam CT measurements of distal tibio-fibular syndesmosis in asymptomatic uninjured ankles: does weight-bearing matter? Skeletal Radiol 2019;48(4):583–594.
46. Halonen KS, Mononen ME, Jurvelin JS, Töyräs J, Salo J, Korhonen RK. Deformation of articular cartilage during static loading of a knee joint--experimental and finite element analysis. J Biomech 2014;47(10):2467–2474.
47. Maier J, Black M, Bonaretti S, et al. Comparison of Different Approaches for Measuring Tibial Cartilage Thickness. J Integr Bioinform 2017;14(2):20170015.
48. Grunz J-P, Pennig L, Fieber T, et al. Twin robotic x-ray system in small bone and joint trauma: impact of cone-beam computed tomography on treatment decisions. Eur Radiol 2021;31(6):3600–3609.
49. Dubreuil T, Mouly J, Ltaief-Boudrigua A, et al. Comparison of Cone-Beam Computed Tomography and Multislice Computed Tomography in the Assessment of Extremity Fractures. J Comput Assist Tomogr 2019;43(3):372–378.
50. Myller KAH, Turunen MJ, Honkanen JTJ, et al. In Vivo Contrast-Enhanced Cone Beam CT Provides Quantitative Information on Articular Cartilage and Subchondral Bone. Ann Biomed Eng 2017;45(3):811–818.
51. Houten JK, Nasser R, Baxi N. Clinical assessment of percutaneous lumbar pedicle screw placement using theO-arm multidimensional surgical imaging system. Neurosurgery 2012;70(4):990–995.
52. Sebaaly A, Jouffroy P, Emmanuel Moreau P, Rodaix C, Riouallon G. Intraoperative Cone Beam Tomography and Navigation for Displaced Acetabular Fractures: A Comparative Study. J Orthop Trauma 2018;32(12):612–616.
53. Franke J, von Recum J, Suda AJ, Grützner PA, Wendl K. Intraoperative three-dimensional imaging in the treatment of acute unstable syndesmotic injuries. J Bone Joint Surg Am 2012;94(15):1386–1390.
54. Kiljunen T, Kaasalainen T, Suomalainen A, Kortesniemi M. Dental cone beam CT: A review. Phys Med 2015;31(8):844–860.
55. Egbert N, Cagna DR, Ahuja S, Wicks RA. Accuracy and reliability of stitched cone-beam computed tomography images. Imaging Sci Dent 2015;45(1):41–47.
56. Hu X, Zhong Y, Lai Y, Shen C, Yang K, Jia X. Small animal photon counting cone-beam CT on a preclinical radiation research platform to improve radiation dose calculation accuracy. Phys Med Biol 2022;67(19):195004.
57. Shi L, Lu M, Bennett NR, et al. Characterization and potential applications of a dual-layer flat-panel detector. Med Phys 2020;47(8):3332–3343.
58. Liu SZ, Zhao C, Herbst M, et al. Feasibility of dual-energy cone-beam CT of bone marrow edema using dual-layer flat panel detectors. In: Medical Imaging 2022: Physics of Medical Imaging. SPIE, 2022;46
59. Benz RM, Harder D, Amsler F, et al. Initial Assessment of a Prototype 3D Cone-Beam Computed Tomography System for Imaging of the Lumbar Spine, Evaluating Human Cadaveric Specimens in the Upright Position. Invest Radiol 2018;53(12):714–719.
60. Winn N, Kaur S, Cassar-Pullicino V, Ockendon M. A novel use of cone beam CT: flexion and extension weight-bearing imaging to assess spinal stability. Eur Spine J 2022;31(7):1667–1681.
61. Zhao C, Herbst M, Vogt S, et al. Cone-beam imaging with tilted rotation axis: Method and performance evaluation. Med Phys 2020;47(8):3305–3320.
62. Herbst M, Luckner C, Wicklein J, et al. Misalignment compensation for ultra-high-resolution and fast CBCT acquisitions. In: Medical Imaging 2019: Physics of Medical Imaging. SPIE, 2019;57.
63. Kunz AS, Schmalzl J, Huflage H, et al. Twin Robotic Gantry-Free Cone-Beam CT in Acute Elbow Trauma. Radiology 2023;306(3):e221200.
64. Posadzy M, Desimpel J, Vanhoenacker F. Cone beam CT of the musculoskeletal system: clinical applications. Insights Imaging 2018;9(1):35–45.

65. van den Bergh JP, Szulc P, Cheung AM, Bouxsein M, Engelke K, Chapurlat R. The clinical application of high-resolution peripheral computed tomography (HR-pQCT) in adults: state of the art and future directions. Osteoporos Int 2021;32(8):1465–1485.
66. de Charry C, Boutroy S, Ellouz R, et al. Clinical cone beam computed tomography compared to high-resolution peripheral computed tomography in the assessment of distal radius bone. Osteoporos Int 2016;27(10):3073–3082.
67. Klose-Jensen R, Tse JJ, Keller KK, et al. High-Resolution Peripheral Quantitative Computed Tomography for Bone Evaluation in Inflammatory Rheumatic Disease. Front Med (Lausanne) 2020;7:337.
68. Michalak GJ, Walker R, Boyd SK. Concurrent Assessment of Cartilage Morphology and Bone Microarchitecture in the Human Knee Using Contrast-Enhanced HR-pQCT Imaging. J Clin Densitom 2019;22(1):74–85.
69. Lu S, Fuggle NR, Westbury LD, et al. Machine learning applied to HR-pQCT images improves fracture discrimination provided by DXA and clinical risk factors. Bone 2023;168:116653.
70. Oostveen LJ, Boedeker KL, Brink M, Prokop M, de Lange F, Sechopoulos I. Physical evaluation of an ultra-high-resolution CT scanner. Eur Radiol 2020;30(5):2552–2560. [Published correction appears in Eur Radiol 2020;30:4709-4710.]
71. Shi G, Subramanian S, Cao Q, Demehri S, Siewerdsen JH, Zbijewski W. Application of a novel ultra-high resolution multi-detector CT in quantitative imaging of trabecular microstructure. In: Medical Imaging 2020: Biomedical Applications in Molecular, Structural, and Functional Imaging. SPIE, 2020;50.
72. Rajendran K, Petersilka M, Henning A, et al. Full field-of-view, high-resolution, photon-counting detector CT: technical assessment and initial patient experience. Phys Med Biol 2021;66(20):205019.
73. Leng S, Bruesewitz M, Tao S, et al. Photon-counting Detector CT: System Design and Clinical Applications of an Emerging Technology. RadioGraphics 2019;39(3):729–743.
74. Si-Mohamed S, Cormode DP, Bar-Ness D, et al. Evaluation of spectral photon counting computed tomography K-edge imaging for determination of gold nanoparticle biodistribution *in vivo*. Nanoscale 2017;9(46):18246–18257.
75. Rajendran K, Baffour F, Powell G, et al. Improved visualization of the wrist at lower radiation dose with photon-counting-detector CT. Skeletal Radiol 2023;52(1):23–29.
76. Booij R, Kämmerling NF, Oei EHG, Persson A, Tesselaar E. Assessment of visibility of bone structures in the wrist using normal and half of the radiation dose with photon-counting detector CT. Eur J Radiol 2023;159:110662.
77. Rau A, Straehle J, Stein T, et al. Photon-Counting Computed Tomography (PC-CT) of the spine: impact on diagnostic confidence and radiation dose. Eur Radiol 2023. 10.1007/s00330-023-09511-5. Published online March 9, 2023.
78. Skelley NW, Smith MJ, Ma R, Cook JL. Three-dimensional Printing Technology in Orthopaedics. J Am Acad Orthop Surg 2019;27(24):918–925.
79. Xiao K, Xu B, Ding L, et al. Traditional versus mirror three-dimensional printing technology for isolated acetabular fractures: a retrospective study with a median follow-up of 25 months. J Int Med Res 2021;49(6):3000605211028554.
80. Tam MD, Laycock SD, Bell D, Chojnowski A. 3-D printout of a DICOM file to aid surgical planning in a 6 year old patient with a large scapular osteochondroma complicating congenital diaphyseal aclasia. J Radiol Case Rep 2012;6(1):31–37.
81. Weidert S, Andress S, Linhart C, et al. 3D printing method for next-day acetabular fracture surgery using a surface filtering pipeline: feasibility and 1-year clinical results. Int J CARS 2020;15(3):565–575. [Published correction appears in Int J CARS 2021;16:703–704.].
82. Choi Y, Jang YJ, Kim KB, Bahng J, Choi SH. Characterization of Tissue Equivalent Materials Using 3D Printing for Patient-Specific DQA in Radiation Therapy. Appl Sci (Basel) 2022;12(19):9768.
83. Binder JS, Scholz M, Ellmann S, et al. Cinematic Rendering in Anatomy: A Crossover Study Comparing a Novel 3D Reconstruction Technique to Conventional Computed Tomography. Anat Sci Educ 2021;14(1):22–31.
84. Rowe SP, Fritz J, Fishman EK. CT evaluation of musculoskeletal trauma: initial experience with cinematic rendering. Emerg Radiol 2018;25(1):93–101.
85. Burns JE, Yao J, Muñoz H, Summers RM. Automated Detection, Localization, and Classification of Traumatic Vertebral Body Fractures in the Thoracic and Lumbar Spine at CT. Radiology 2016;278(1):64–73.
86. Burns JE, Yao J, Wiese TS, Muñoz HE, Jones EC, Summers RM. Automated detection of sclerotic metastases in the thoracolumbar spine at CT. Radiology 2013;268(1):69–78.
87. Kalia V, Obray RW, Filice R, Fayad LM, Murphy K, Carrino JA. Functional joint imaging using 256-MDCT: Technical feasibility. AJR Am J Roentgenol 2009;192(6):W295–W299.
88. Flohr TG, McCollough CH, Bruder H, et al. First performance evaluation of a dual-source CT (DSCT) system. Eur Radiol 2006;16(2):256–268.
89. Lenga L, Leithner D, Peterke JL, et al. Comparison of Radiation Dose and Image Quality of Contrast-Enhanced Dual-Source CT of the Chest: Single-Versus Dual-Energy and Second-Versus Third-Generation Technology. AJR Am J Roentgenol 2019;212(4):741–747.
90. Drake MT. Osteoporosis and cancer. Curr Osteoporos Rep 2013;11(3):163–170.
91. Taguchi K, Itoh T, Fuld MK, Fournie E, Lee O, Noguchi K. "X-Map 2.0" for Edema Signal Enhancement for Acute Ischemic Stroke Using Non-Contrast-Enhanced Dual-Energy Computed Tomography. Invest Radiol 2018;53(7):432–439.